ACS MATERIALS Au
AN OPEN ACCESS JOURNAL OF THE AMERICAN CHEMICAL SOCIETY

pubs.acs.org/materialsau
Article

Realizing the Potential of Commercial E-Textiles for Wearable Glucose Biosensing Application

Moshfiq-Us-Saleheen Chowdhury, Sutirtha Roy, Krishna Prasad Aryal, Henry Leung, and Richa Pandey*

Cite This: ACS Mater. Au 2024, 4, 592−603
Read Online
ACCESS | Metrics & More | Article Recommendations | Supporting Information

ABSTRACT: Advancements in wearable technology have enabled noninvasive health monitoring using biosensors. This research focuses on developing a textile-based sweat glucose sensor using commercially available conductive textiles, evading the complexity of traditional fabrication methods. A comparative analysis of three low-cost conductive textiles, Adafruit 1364, 1167, and 4762, has been conducted for electrochemical glucose detection with glucose-specific enzymes such as glucose oxidase (GOx) and glucose dehydrogenase (GDH). Adafruit 1364 outperformed others in morphological, electrochemical, and wearable properties. Cyclic voltammetry shows that Adafruit 1364 and 4762 effectively detect glucose at the potential of 0.23 and 0.08 V using glucose oxidase and 0.1 and 0.08 V using glucose dehydrogenase enzymes, respectively. Furthermore, chronoamperometry has been conducted to confirm the presence of glucose at 1 μM concentration. Differential pulse voltammetry was conducted to assess the sensitivity of the Adafruit 1364 fabric electrode using glucose solutions with concentrations of 0.05, 0.15, 0.25, and 0.5 mM. The electrode immobilized with GOx showed a sensitivity of 0.005 μA μM^{-1} and a limit of detection (LOD) of 41.3 μM, while the electrode immobilized with GDH exhibited a sensitivity of 0.0019 μA μM^{-1} and an LOD of 63.1 μM. The study also highlighted the reproducibility, effect of interferents, and advantageous wearable properties of these sensors.

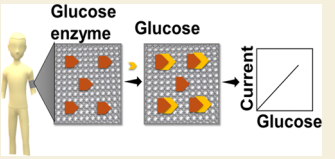

KEYWORDS: *chronoamperometry, electrochemical sensing, e-textiles, glucose, wearable device*

1. INTRODUCTION

Sensors made from textiles are an exciting blend of old-school fabric making and new-age sensor technology, resulting in the emergence of the term "smart textiles". Smart textiles also referred to as smart fabrics or e-textiles are pieces of fabrics integrated with electronic components for applications in medical devices,[1] fitness trackers,[2] therapeutic clothing,[3] fashion and design,[4] military and defense,[5] etc. E-textiles are of special interest in wearable applications to track different physical and health-related measurements.[2] By weaving,[6] stitching,[7] printing,[8] or applying a special coating,[9] these sensors are added directly to the cloth, making it possible to turn regular clothing and accessories into high-tech wearables. This innovative technique is a game changer in wearable technologies, allowing for better health tracking and enhancement of athletic performance.

Textile-based sensors are usually fabricated with e-textiles and made by adding conductive materials into cloth, which changes the way we think about wearable devices and smart clothing. They play a crucial role in the development of smart clothing, allowing for the integration of sensors and actuators to monitor physiological parameters and enhance the user experience. Additionally, these textiles are utilized for generating controlled heat,[10] ensuring comfort and safety in cold environments. Moreover, their conductive properties enable electromagnetic interference shielding, safeguarding sensitive electronic equipment.[11,12] The sensors made from conductive or e-textiles work by detecting physical, chemical, or biochemical changes around them and turning these changes into electrical signals that we can measure and understand. They are made to detect many different parameters, such as heat,[13−17] pressure,[18−23] strain,[24−28] humidity,[29,30] and various chemicals.[31,32] These sensors fit well to the various shapes of the human body, making them perfect for constantly checking on health measurements and physical movements without causing any discomfort or intrusion.[1,2] Since their first appearance, there have been major improvements in the area of textile sensors.[33] Researchers have been experimenting with different kinds of conductive materials, including metal threads,[34] conductive materials,[35,36] and graphene[37−42] to fabricate e-textile-based sensors for different applications. They aim to make these sensors not only more efficient but also stronger and more comfortable to wear. Till now, complex and time-consuming fabrication processes like dip coating of threads and weaving have been utilized for creating e-textiles.[43] New methods like three-dimensional (3D) printing[8,44,45] and nanotechnology[46,47] have also improved these sensors' performances, making them

Received: May 8, 2024
Revised: July 11, 2024
Accepted: July 15, 2024
Published: July 23, 2024

more sensitive and susceptible to multiple applications and producing clearer signals.

An important breakthrough is the use of these e-textile sensors in tracking health.[48−51] They can continuously check important health indicators such as heart rate,[52,53] breathing rates,[54] and body temperature.[55] There have also been steps forward in sensors that monitor the movement and body position,[56,57] which can be used for athletes to get better at their sports and people getting physical therapy.

Glucose detection in biological fluids has extended beyond diabetes care, branching into broader health monitoring and well-being tracking such as tracking endocrine disorder,[58] nutritional status,[59] energy balance,[60] etc. Wearable glucose sensors offer a real-time means for individuals to monitor their glucose levels, offering valuable insights into metabolic health and aiding in the early identification of possible health concerns. Through the integration of glucose-sensitive bioreceptors or chemical receptors into textiles, for example, the incorporation of carbon nanotubes,[10] organic compounds such as pyrrole,[61] or microfluidic channels,[62] the intelligent fabrics can detect fluctuations in glucose levels via interactions with bodily fluids or sweat. Subsequently, the information gathered by these sensors can be wirelessly transmitted to external devices or smartphones, enabling real-time monitoring and analysis. So far, significant effort has been made developing methods to detect glucose using textiles. A review of these methods including the results of our proposed fabric electrode is detailed in Table S1 in the Supplementary Information section.

This research examines the potential of commercially available, low-cost e-textiles for the electrochemical detection of glucose. The commercial fabrics were investigated for their wearable properties and bioreceptor (glucose oxidase and glucose dehydrogenase) integration. The fabricated e-textile-based glucose biosensors demonstrated the sensitive detection of glucose.

2. METHODS AND MATERIALS

2.1. Materials

For this research, three commercially available and cost-effective conductive textiles were selected, which are Sample 1: Adafruit 1364 (KNIT JERSEY conductive fabric), Sample 2: Adafruit 1167 (KNIT conductive fabric silver); and Sample 3: Adafruit 4762 (NYLON fabric squares with conductive adhesive). All three samples are innovative products from Adafruit Industries, specifically designed to meet the increasing demand for conductive textiles in the domains of electronics and wearables. Ag/AgCl reference electrodes (CH instruments) and platinum wire counter electrodes (CH instruments) were used as reference and counter electrodes, respectively, whereas potassium hexacyanoferrate(II) ($K_4[Fe(CN)_6]$) (ACS reagent, 98.5−102.0%, Sigma-Aldrich), sodium chloride (NaCl) (ACS reagent, ≥99.0%, Sigma-Aldrich), and phosphate buffer solution (PB) (1.0 M, pH 7.4,Sigma-Aldrich) were used to make electrolytic solution for the electrochemical tests (cyclic voltammetry and electrochemical impedance spectroscopy) to validate the electrochemical properties of the samples. Glucose oxidase (GOx) from *Aspergillus niger* (≥100,000 units/g solid, Sigma-Aldrich) and glucose dehydrogenase (GDH) from Pseudomonas sp. (≥200 U/mg solid, Sigma-Aldrich) were used in the glucose sensing test.

2.2. Electrode Fabrication and Testing

A poly(ethylene terephthalate) (PET) sheet was cleaned with isopropyl alcohol (IPA) to be used as a base layer for each fabric to make them rigid for testing. Each of the fabric samples was precisely cut into sample electrodes measuring 40 mm × 10 mm manually. 2 mM potassium hexacyanoferrate(II) trihydrate solution was used as an electrolytic solution for investigating the electrochemical properties of the electrodes. 50 μL of 1 μM GOx solution was drop-cast on the 0.5 × 0.5 cm area of the samples for glucose sensing. To specify this area for the enzyme's electrochemical reaction with glucose, an insulation mark was created using regular nail polish. 50 μL of 0.16 mg/mL GDH was deposited on a separate batch of the fabric electrode in order to conduct a similar test.

2.3. Characterization

2.3.1. Physical Characterization. In order to assess the physical characteristics of the fabrics, scanning electron microscopy (SEM) and energy-dispersive X-ray spectroscopy (EDS) were used to analyze the morphological structure of the fabrics and its material composition. In addition to that, the surface absorptivity, tensile strength, and electrical properties have also been analyzed. To understand the material characteristics of each fabric, SEM and EDS analyses were conducted for each sample using a backscattered electron detector desktop SEM (Phenom Pro X, Thermo Fisher Scientific) with a scale of 50 μm for Adafruit 1167, 100 μm for Adafruit 4762, and 200 μm for Adafruit 1364 to get a suitable morphological view. The scales differed since all three samples had different morphological structures. The surface absorptivity of Adafruit 1364, 1167, and 4762 was evaluated by dispensing 100 μL of distilled water onto the surface. Subsequently, the contact angle of the water droplet was recorded for 800 s using a contact angle analysis machine (OCA15EC optical contact angle & contour analysis system, Dataphysics) to determine the surface absorptivity of the samples precisely. For analyzing the tensile strength of the samples, each sample was placed on a mechanical testing machine (UniVert, Cell Scale), and a range of force (0−50 N) was applied to check the breakpoint of each sample. The sheet resistance of each sample was measured to analyze their electrical properties. For sheet resistance analysis, a 4-point probe measurement was conducted using a four-point probe (Four-Point Probe, Ossila). The experimental setup involved a probe equipped with four uniformly positioned electrical contacts (needles or pins) establishing direct contact with the material under examination. By applying Ohm's law ($V = I * R$), the sheet resistance (R) of the material was computed using measured voltage and current values. An initial aspect ratio of 0.25 was kept for all three samples prior to the test and afterward, all the samples were manually stretched up to 20% of their dimension to see the change in the sheet resistance.

2.3.2. Electrochemical Characterization. To examine the electrochemical properties of the materials, comprehensive analyses were conducted using cyclic voltage (CV) and electrochemical impedance spectroscopy (EIS). The experimental setup included three fabric sample types serving as working electrodes, with Ag/AgCl and platinum electrodes utilized as the reference and counter electrodes, respectively. 2 mM potassium hexacyanoferrate(II) trihydrate solution served as the electrolyte. For CV, the applied potential to the working electrode underwent a linear sweep across −0.4 to 0.4 V, for the scan rates varied from 0.02 to 0.2 V using a potentiostat (Emstat 4s, Palmsens). For EIS, a potential of 0.006 V was applied over the range of frequency of 0.05−5000 Hz using the same potentiostat (Emstat 4s, Palmsens). Subsequently, the impedance spectrum was analyzed by fitting it to an equivalent circuit model using software (PSTrace 5.9, Palmsens). To evaluate the ability of the fabrics to detect glucose, chronoamperometry has been done. CV was done with the same setup as mentioned in the previous subsection but with four different electrolytes (4 mL of 1 mM PB, 4 mL of 1 μM glucose, 4 mL of 1 μM GOx, and 4 mL of a mixture of 2 mL of 1 μM glucose and 2 mL of 1 μM GOx) to figure out the anodic or cathodic peak voltages. The GOx- and GDH-deposited electrodes were measured using chronoamperometry in 4 mL of 25:25 buffer as an electrolyte. Chronoamperometry with GOx-deposited electrodes was conducted with applied voltages of 0.23 V for Adafruit 1364, 0.22 V for Adafruit 1167, and 0.08 V for Adafruit 4762. For GDH-deposited electrodes, the chronoamperometry was conducted at a voltage of 0.1 V for Adafruit 1364, 0.16 V for Adafruit 1167, and 0.08

https://doi.org/10.1021/acsmaterialsau.4c00033
ACS Mater. Au 2024, 4, 592−603

V for Adafruit 4762. The electrode responses were recorded for 1000 s, and within the initial 700 s, 100 μL of 1 μM glucose solution was added at 100 s intervals to observe the current response of the electrodes using software (PSTrace 5.9, Plamsens). The current response was recorded by observing the increase of current at the time (t = 102 s) when the glucose solution was first added and current at the end of the experiment (t = 1000 s). With the Adafruit 1364 fabric electrode giving the best result in chronoamperometry, differential pulse voltammetry (DPV) was done with multiple concentrations of glucose (0, 0.05, 0.15, 0.25, and 0.5 mM) in 1 mM phosphate buffer solution to calculate the sensitivity (the slope of the calibration curve) and limit of detection ((3*standard deviation of current in blank state)/sensitivity).[63,64] The sensor lifetime and reproducibility were observed by calculating the standard deviation of the current. First, the DPV was conducted using GOx- and GDH-immobilized Adafruit 1364 fabric electrodes with 0.05 mM glucose, and the electrode was kept at room temperature (24 °C) for 4 and 8 h of intervals in a Petri dish. After each interval, DPV was repeated with the same glucose concentration solution, and the current was recorded for calculating the standard deviation. Finally, the effect of interference was studied by performing DPV on the surface of the Adafruit 1364 electrode containing immobilized GOx and GDH. The study included adding 1 mM lactic acid and 1 mM ascorbic acid to the 1 mM glucose solution. After the addition of each interferant, the solution was mixed properly.

3. RESULTS AND DISCUSSION

The schematic illustration in Figure 1A shows the overall concept of commercial e-textiles used in wearable glucose biosensing applications. For detecting any bioparameters, out of the e-textile, any armband or similar clothing can be made and worn. Specific enzymes will be deposited on the clothing as shown in Figure 1B, which will initiate an enzymatic reaction with a definite biomarker of sweat or any body fluids giving signals of its presence. The methodology for biomarker detection, specifically targeting glucose in this research, is also depicted in Figure 1B. The enzymes, both GOx and GDH, oxidized the glucose and produce hydrogen peroxide (in the case of GOx) and reduced the state of GDH (for GDH) as byproducts, resulting in an augmented electrical current that facilitates the identification of the glucose. In Table 1, the summary of investigations done in this research has been highlighted.

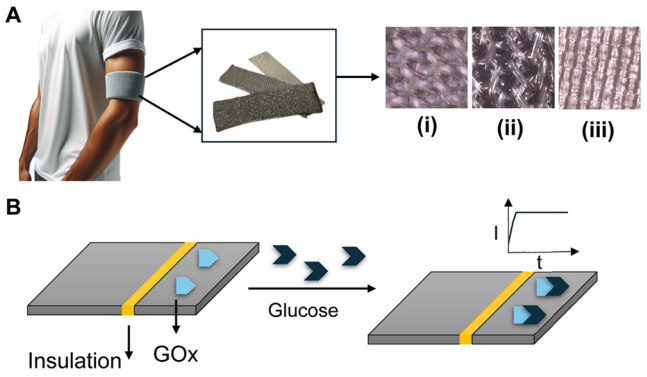

Figure 1. Schematic illustration of (A) concept of e-textiles to be used as wearable glucose biosensors, where (i), (ii), and (iii) represent a microscopic view of Adafruit 1364, 1167, and 4762, respectively. (B) Electrode fabrication and glucose detection on the e-textile-integrated specific glucose enzymes. The authors have used an open-source platform (DALL-E) to generate the arm image used in Figure 1A.

Table 1. Summary of Investigations

analysis	technique	purpose of study
physical properties	scanning electron microscopy (SEM)	morphological analysis
	energy-dispersive X-ray spectroscopy (EDS)	morphological analysis
	tensile strength	strength of the fabric to withstand load
	optical contact angle measurement	surface absorptivity
	4-point probe measurement	surface resistance
electrochemical properties	cyclic voltammetry	electrochemical performance
	electrochemical impedance spectroscopy	charge transfer resistance, solution resistance, double-layer capacitance calculation
	chronoamperometry	glucose detection
	differential pulse voltammetry	glucose detection, sensitivity calculation, reproducibility and effect of interferent study

3.1. Material Characterization

Figure 2 illustrates the SEM and EDS analyses that were conducted on all three fabric samples investigated in this research. Since all the fabrics have different structures, to get a detailed idea of the morphology of each material, each fabric has been analyzed in different magnification factors. The SEM images on a scale of 200 μm of the first sample (Figure 2A) reveal the presence of two distinct types of cylindrical strands, with the darker strand having a diameter of 7.46 μm and the lighter strand having a diameter of approximately 21.9 μm. This observation suggests that Adafruit 1364 is composed of a combination of at least two different materials. Figure 2B illustrates the SEM image of Adafruit 1167 at a scale of 50 μm, exhibiting a lighter, flat strand with a width of approximately 23.1 μm. Figure 2C provides insights into the structure of Adafruit 4762 at a scale of 100 μm, revealing strongly attached cross-linked strand sites with a width of approximately 13.8 μm each and a compact structure. Following the morphological analysis, elemental composition identification was performed.

The in situ image of Figure 2A represents the component mapping of Adafruit 1364, which shows the sample consisting of a balanced distribution of silver, carbon, and oxygen. The lighter strands in the specimen show the presence of silver, which is considered to contribute to the conductivity of the sample.

The in situ image of Figure 2B represents the composition mapping of Adafruit 1167; here, the strands have silver, carbon, and nitrogen disposed together. This might result in the sample working as a nitrogen-doped material with the possibility of having higher capacitive behavior.[65] Adafruit 4762 has a compact morphological structure with an abundance of nickel and copper as per the in situ image in Figure 2C. Due to having a compact structure, the electrochemical interactivity of Adafruit 4762 should be less compared to other samples.

Figure S1 displays the detailed elemental composition mapping of each material. The mapping shows that both Adafruit 1364 and 1167 contain abundant silver and carbon with Adafruit 1167 exhibiting a higher silver composition. This implies that both specimens should demonstrate equivalent or similar electrochemical characteristics, resembling those of an ideal silver electrode. The weight concentration percentages for Adafruit 1364 are 39.07, 36.44, and 24.49% for silver,

https://doi.org/10.1021/acsmaterialsau.4c00033
ACS Mater. Au 2024, 4, 592−603

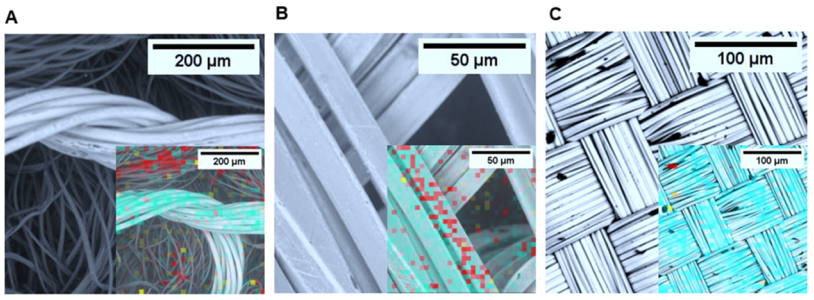

Figure 2. (A) Scanning electron microscopy (SEM) of Adafruit 1364 (KNIT JERSEY Conductive Fabric); in situ image represents the component mapping of Adafruit 1364, where the blue region represents the presence of silver (Ag), red represents carbon (C), and yellow represents oxygen (O), (B) SEM of Adafruit 1167 (KNIT conductive fabric silver); in situ image represents the component mapping of Adafruit 1167, where the blue region represents the presence of silver (Ag), red represents carbon (C) and nitrogen (N), and yellow represents oxygen (O), and (C) SEM of Adafruit 4762 (NYLON fabric squares with conductive adhesive); in situ image represents the component mapping of Adafruit 4762, where the blue region represents the presence of nickel (Ni), red represents carbon (C) and nitrogen (N), yellow represents oxygen (O), and orange represents copper (Cu).

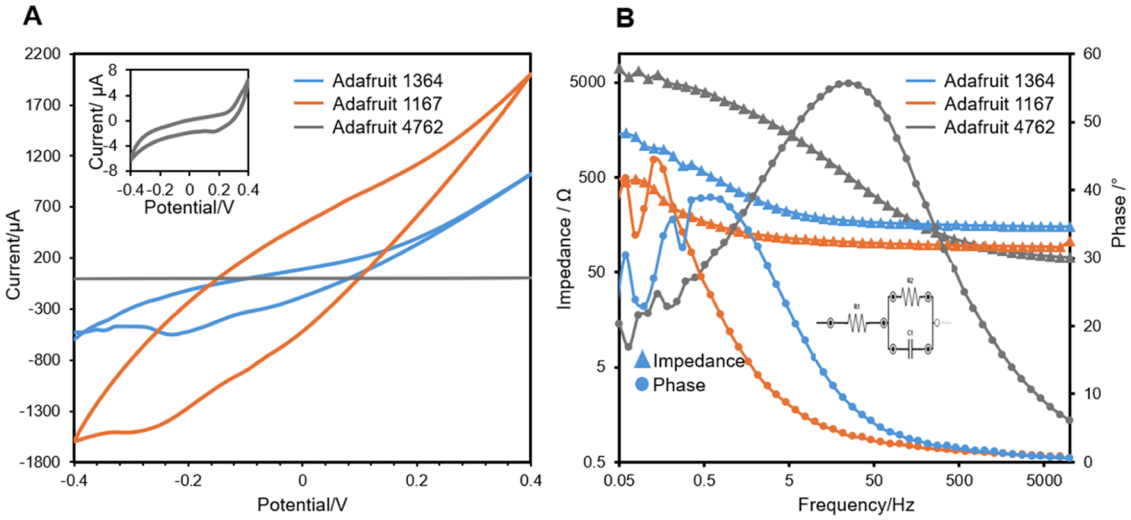

Figure 3. (A) Cyclic voltammetry; the in situ image represents cyclic voltammetry of Adafruit 4762. (B) Electrochemical impedance spectroscopy of Adafruit 1364, 1167, and 4762; the in situ image represents the equivalent circuit for circuit fitting.

carbon, and oxygen, respectively. In contrast, Adafruit 1167 displays weight concentration percentages of 49.94, 28.54, and 9.86% for silver, carbon, and oxygen, along with 11.65% nitrogen, respectively. This divergence of 11.65% nitrogen in Adafruit 1167 may alter the electrochemical characteristics of the sample compared to that of an ideal silver electrode.[65] Adafruit 4762 exhibits an abundant amount of nickel and a slight amount of copper with weight concentration percentages of 80.18 and 9.69%, respectively. This suggests that Adafruit 4762 is likely to manifest different electrochemical properties compared to those of Adafruit 1364 and 1167. Additionally, traces of carbon, oxygen, and nitrogen are present in Adafruit 4762, along with traces of copper oxide (CuO), which could generate additional byproducts during electrochemical characteristics of the sample (Figure S2).

Figure 3A showcases the CV responses of three samples using a 2 mM potassium hexacyanoferrate(II) solution as an electrolyte, providing insights into their electrochemical properties. The analysis focuses on discerning the occurrence of irreversible reactions and understanding the capacitive current exhibited by Adafruit 1167, which is expected since the capacitive properties of the sample should be high due to the porous nature of the fabric, which can be seen through the optical contact angle measurement results and the presence of nitrogen and its functionality being almost similar to nitrogen-doped carbon materials.[65] The introduction of nitrogen may enhance reaction kinetics, resulting in elevated nonfaradaic currents for Adafruit 1167.[65] The curves depicted in Figure 3A unveil a subtle cathodic peak at −0.21 V for Adafruit 1364, −0.27 V for Adafruit 1167, and 0.18 V for Adafruit 4762, suggesting that the electrochemical procedure primarily entails reduction of Fe^{2+} within the potential sweep range of −0.4 to 0.4 V. Following CV, peak cathodic currents for each sample were calculated and plotted against the square root of scan rate (Figure S3) to assess their conformity to the Randles−Sevcik equation[66,67] (eq i), which is

$$I_p = 2.69 \times 10^5 N^{3/2} A c \sqrt{D\nu} \quad \text{(i)}$$

where

I_p = current maximum in amps

N = number of electrons transferred in the redox event (usually 1)

A = area of the electrode in cm^2

D = diffusion coefficient in cm^2/s

c = concentration in mol/cm^3

ν = scan rate in V/s

https://doi.org/10.1021/acsmaterialsau.4c00033
ACS Mater. Au 2024, 4, 592−603

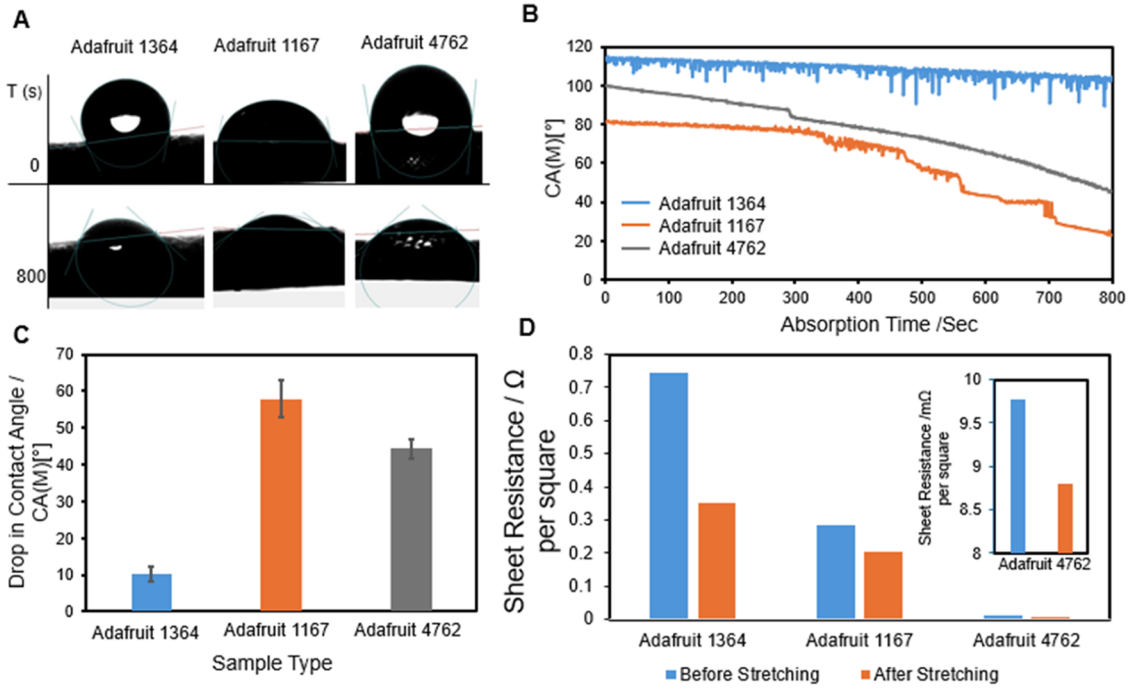

Figure 4. (A) Optical water contact angle images of Adafruit 1364, 1167, and 4762. (B) Measured dynamic contact angle of water droplets on the surfaces for 800 s. (C) Drop in the optical contact angle with respect to time for each sample. (D) Sheet resistance of each sample before and after stretching; the in situ image represents sheet resistance before and after stretching for Adafruit 4762.

Adafruit 1364 and 4762 conform to the expectations of the Randles−Sevcik equation, showcasing an increase in the cathodic peak currents with an escalating square root of the scan rate. The cathodic peak current for Adafruit 4762 is quite less compared to 1364. It may be due to the presence of nickel, which is electrochemically less reactive than silver because of their stable oxidation state (Ni^{2+}) and reluctance to go through any oxidation or reduction reaction. Adafruit 1167 deviates from this trend. The observed deviation in the behavior of Adafruit 1167 is attributed to the influence of the material composition discussed in the preceding sections. Due to an increase in scan rate, the capacitive current increases in the electrochemical reactions.[68] The presence of a more capacitive nature in the material will cause the nonfaradaic current to mask over the faradaic current, resulting in a decrease in the faradaic peaks with increasing scan rate. The presence of a capacitive nature and deviations from the Randles−Sevcik equation suggest that Adafruit 1167 may not be an optimal choice for electrochemical processes.[69,70]

Figure 3B presents the Bode plot of the EIS for all three samples, unraveling distinctive features in charge transfer resistance. The charge transfer resistance and double-layer capacitance were calculated by designing a Randles circuit with a constant-phase element (CPE) (Table S2) using software (PSTrace 5.9, Plamsens). Adafruit 4762 exhibits the highest charge transfer resistance, approximately 3910.67 Ω, followed by Adafruit 1364 with approximately 1265.67 Ω and Adafruit 1167 displaying the least resistance at 927.5 Ω. On the contrary, the solution resistances are 172.83, 109.43, and 100.67 Ω for Adafruit 1364, 1167, and 4762, respectively. This observation suggests that Adafruit 1167 manifests the fastest electron transfer, reflecting its favorable characteristics for efficient electrochemical processes.

Contrastingly, the double-layer capacitance values reveal a different aspect. Adafruit 1167, while demonstrating the lowest charge transfer resistance, also exhibits the highest double-layer capacitance at approximately 1000 μF. In comparison, Adafruit 1364 and sample 4762 have capacitance values of 606.86 and 24.90 μF, respectively. The elevated double-layer capacitance in Adafruit 1167 implies unwanted capacitive contributions, potentially interfering with specific electrochemical processes or signals, which have been seen as the increased nonfaradaic current in the cyclic voltammetry curve. Notably, Adafruit 4762 showcases the least unwanted double-layer capacitance, an essential characteristic for an ideal electrode in biosensor applications. However, it concurrently presents the maximum charge transfer resistance. In contrast, Adafruit 1364 strikes a balance, featuring an optimum charge transfer resistance and a commendable dual charge capacitance.

The performance of the fabrics also depends on the porosity of the surface. Adafruit 1364 contains cotton, whereas on the other hand, Adafruit 4762 contains nylon. Cotton fibers are natural and composed of cellulose, which gives them an inherently open and porous structure. This high porosity enables cotton to absorb moisture effectively, making it breathable and comfortable for use in clothing and other fabrics. In contrast, nylon is a synthetic fiber with a more compact molecular structure, leading to a lower porosity. As a result, nylon fabrics are less breathable and absorbent than cotton, making them more water-resistant.[71,72] Due to its cotton content, Adafruit 1364 exhibits higher porosity, which enhances its participation in electrochemical reactions compared to the compact nylon structure of Adafruit 4762.

3.2. Wearable Characteristics

To validate the surface absorptivity of the e-textile for sweat or water, contact angle measurements were performed. At time T = 0 s, the contact angles of the droplets for Adafruit 1364, 1167, and 4762 were 114.46, 81.02, and 99.53°, respectively. After 800 s, these angles decreased to 104.10, 23.15, and

https://doi.org/10.1021/acsmaterialsau.4c00033
ACS Mater. Au 2024, 4, 592−603

55.26°, respectively (Figure 4A). Figure 4B presents a curve illustrating the drop in the contact angle of the droplet over time. Figure 4C highlights that the droplet on Adafruit 1364 experienced the least decrease in the contact angle. This implies that for Adafruit 1364, the sweat or biological sample will linger on the surface for an extended duration compared to 1167 and 4762, providing ample time for proper electrochemical reactions. On the surface of Adafruit 1167, the droplet disperses quickly due to which the analyte has less chance to accumulate over its surface. This quick drop also provides insights regarding the presence of pores on the surface of the fabric, which also exerts an effect on the electrochemical interactions. On the contrary, since the dispersion time for 1364 is longer, the analytes have better chances to remain anchored onto the surface of the fabric. In the case of Adafruit 4762, although the droplet disperses rapidly, it is not absorbed into the fabric; the solution is observed to disperse over the surface instead. Generally, the response time for enzymes to react with glucose takes 2−3 s,[73] but this also varies concerning the concentration of enzymes/glucose, temperature, and pH of the surrounding. Considering that the fabric will be employed as potential biosensors for sweat analysis, involving prolonged skin contact, a moderate to low absorptivity (as seen in Adafruit 1364) may be deemed suitable to strike a balance between comfort and functionality.

In the realm of electrical conductivity, Adafruit 1364 presents a considerable variability in its sheet resistance when subjected to four-point probe measurements. Remarkably, the sheet resistance of the fabric experiences a sharp decline (approximately by 60%) upon stretching, as illustrated in Figure 4D. Such pronounced variations pose significant challenges like inconsistency in performance, heat generation due to drop in resistance, and higher current flow and calibration issues when integrating electronic components to fabricate a biosensor. Conversely, both Adafruit 1167 and 4762 exhibit a gradual reduction in sheet resistance (approximately 33 and 9%, respectively) under similar stretching conditions. Additionally, as mentioned earlier, the samples underwent manual stretching to 20% of their original size to facilitate experimentation. It was observed that both 1364 and 1167 displayed ease of stretchability, while Adafruit 4762 exhibited limited stretchability, reaching a maximum increase in the geometric area of only 5%. The structural configuration of strongly attached cross-linked strands, as identified in the Material Characterization subsection, is speculated to be the contributing factor behind the constrained stretchability observed in Adafruit 4762. This observation aligns with the findings from the surface absorptivity experiment, where the solution droplet on Adafruit 4762 accumulated on the fabric's surface rather than being absorbed. These insights not only shed light on the mechanical properties of the samples but also underscore the critical interplay among the material structure, stretchability, and electronic integration challenges in the context of biosensor development.

The durability of the samples was examined by using a tensile strength test. In Figure S4, the graph showing force against displacement illustrates the robustness of each material. Force was applied until no visible stress was detected in the materials. Once strain became apparent, an optimized force was maintained. The experiment lasted for 275 s. Adafruit 1167 and 4762 failed at times of 201 and 52 s when subjected to maximum forces from 0−15 N and 0−52 N with an extension of 19 and 5 mm, respectively. Adafruit 1364, in contrast, managed to withstand a force close to 18 N with a displacement of 15 mm. It is evident that when pressure is applied, Adafruit 1167 and 4762 are prone to breaking, whereas Adafruit 1364 attempts to maintain its integrity. This demonstrates that Adafruit 1364 is not only elastic but also possesses considerable strength akin to that of the fabric. For a wearable sensor patch, it is crucial to endure both adhesion to the skin and mechanical stress, such as stretching and bending. Tensile strength testing reveals the fabric's capacity to withstand forces significantly higher than those typically encountered in wearable applications.

As mentioned, a constant force was applied over the samples until strain was observed. For Adafruit 4762, due to the compact structure as discussed in the previous section, the tensile strength was increased continuously until there was a minimum strain of 1 mm due to which even at 3.5 times applied tensile strength in comparison to Adafruit 1167, the sample faced only a strain of 5 mm. This implies that Adafruit 1364 and 1167 possess good stretchability compared to 4762, whereas 1167 is less stretchable than 1364 by 35% (force/displacement).

3.3. Real-Time Glucose Sensing

Following a comprehensive analysis of the electrochemical properties of the three fabrics, an assessment of their suitability for use as biosensors was conducted through a proof-of-concept glucose sensing test. This evaluation aimed to gauge the compatibility of the sensors for potential application in sweat glucose monitoring; glucose oxidase and glucose dehydrogenase, two pivotal enzymes known for their specificity in catalyzing the oxidation of glucose, were immobilized onto the surfaces of the test samples. Subsequently, chronoamperometry was employed to record the current response of each sample under the influence of glucose oxidase and glucose dehydrogenase.

In the enzymatic reaction where GOx interacts with glucose, the enzyme facilitates the conversion of both α and β forms of glucose into gluconic acid and hydrogen peroxide (H_2O_2), a process characterized by electron transfer from glucose to molecular oxygen (O_2), the latter serving as the electron acceptor. This biochemical reaction is delineated as follows

$$\text{Glucose} + O_2 \rightarrow \text{Gluconic Acid} + H_2O_2 \quad \text{(ii)}$$

Within the framework of a biosensor or an electrochemical apparatus, the GOx-catalyzed reaction is instrumental in producing an electrical signal. The generation of hydrogen peroxide is crucial to this mechanism. This leads to electron movement toward the hydrogen peroxide, resulting in its decomposition into water and oxygen or oxygen and protons.[74]

The transferred electrons contribute to the generation of an electrical current at the electrode surface. Importantly, the rate of electron transfer is directly proportional to the concentration of glucose in the solution. Higher glucose concentrations lead to an increased rate of electron transfer and, consequently, an increased current.

On the contrary, within the interaction between GDH and glucose, the enzymatic action of GDH facilitates the conversion of glucose into gluconolactone. This transformation involves electron migration from the glucose molecule to an electron acceptor, which may be a naturally occurring cofactor, such as nicotinamide adenine dinucleotide (NAD^+) or flavin adenine dinucleotide (FAD^+). The biochemical reaction is delineated below

https://doi.org/10.1021/acsmaterialsau.4c00033
ACS Mater. Au 2024, 4, 592−603

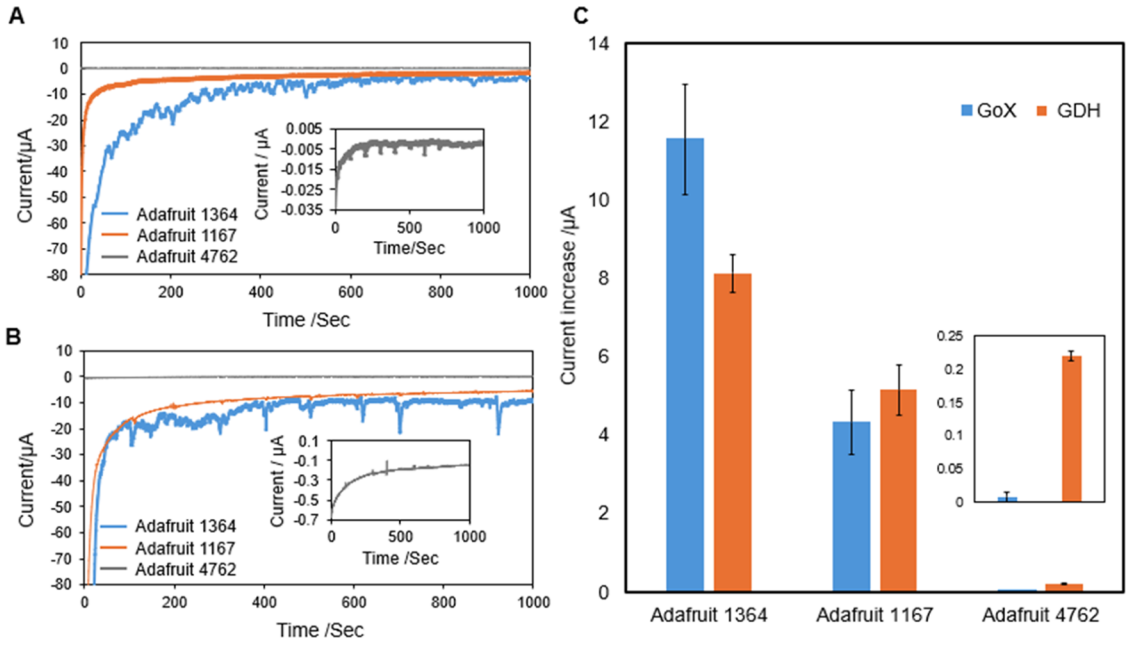

Figure 5. Chronoamperometry of all three samples (A) using glucose oxidase—Adafruit 1364: 0.23 V, Adafruit 1167: 0.22 V, and Adafruit 4762: 0.08 V and (B) using glucose dehydrogenase—Adafruit 1364: 0.1 V, Adafruit 1167: 0.16 V, and Adafruit 4762: 0.08 V. (C) Increase in current after addition of glucose; the in situ image represents chronoamperometry (A) using glucose oxidase and (B) using glucose dehydrogenase and (C) represents an increase in current for Adafruit 4762.

$$\text{Glucose} + \text{GDH} - \text{NAD}^{+} \rightarrow \text{Gluconolactone} + \text{GDH} - \text{NADH} \quad \text{(iii)}$$

In applications involving biosensors or electrochemical apparatuses, this redox reaction is exploited to create an electrical signal. Following the oxidation of glucose, the enzyme in its reduced state (e.g., GDH−$FADH_2$/GDH−$NADH_2$) undergoes reoxidation, during which electrons are transferred to the electrode either directly or via an intermediary mediator chain, dependent on the sensor's architectural design.[75]

In this experiment, no cofactor was utilized, and GDH was directly applied on the electrode surfaces. The morphological analysis in the previous section shows that Adafruit 1167 and 4762 contain a certain amount of nitrogen, which is a key element in the structure of many molecules that work as cofactors of GDH,[76] mimicking a NAD-dependent GDH enzyme over the top of Adafruit 1167 and 4762. On the other hand, Adafruit 1364 does not contain any nitrogen due to which bare GDH current response is quite less compared to that of Adafruit 1167 and 4762. NAD is a cofactor consisting of two nucleotides, adenine and nicotinamide, connected by phosphate groups, and it plays a role in cellular redox reactions. These nucleotides are adenine mononucleotide (AMP) and nicotinamide mononucleotide (NMN). Nicotinamide, derived from niacin (vitamin B3), features a pyridine ring structure with an amide group ($-CONH_2$).[77,78] The nitrogen atom within nicotinamide's pyridine ring is essential for NAD's redox function. NAD is principally involved in redox reactions, transitioning between its oxidized (NAD^+) and reduced (NADH) forms. During these reactions, the nitrogen atom within nicotinamide's ring plays a crucial role in accepting or donating electrons. NAD's ability to accept a hydride ion (H^-) during oxidation reactions is pivotal for its metabolic function. Here, the nitrogen atom of nicotinamide accepts the hydride ion, resulting in the formation of NADH.[76,79,80] Due to this presence of the nitrogen element in the structure of Adafruit 1167 and 4762, the current response of GDH should be more comparable to that of GOx since in the presence of nitrogen, the GDH might work approximately like NAD-dependent GDH.

Figure S5 shows the CV of glucose oxidase with glucose and glucose dehydrogenase for each sample to detect the anodic/cathodic peak voltage of the electrochemical reaction. For GOx-deposited electrodes, the cathodic peaks were observed at 0.23 V for Adafruit 1364 and 0.08 V for Adafruit 4762. It is to be noted that for Adafruit 1167, the double-layer capacitance is high, resulting in no clear peaks, and the peak voltage for a standard silver electrode has been considered. A voltage of 0.22 V was considered for Adafruit 1167 since the cathodic peaks were observed at the same potential in the case of the standard silver electrode. In the case of GDH-deposited electrodes, the cathodic peak voltages were observed at 0.1 V for Adafruit 1364, 0.16 V for Adafruit 1167, and 0.08 V for Adafruit 4762.

Figure 5A and B illustrate the gradual curve depicting the incremental rise in current during the experiment using GOx- and GDH-deposited electrodes, respectively. Notably, drops of 1 μM glucose were drop-cast at specific time intervals, with the first drop occurring between t = 100−120 s and the last drop placed at t = 700−720 s. Figure 5C summarizes the overall increased current observed after the experiment. The figure shows that the increase in current in the case of GDH-applied electrodes is higher compared to that of GOx-applied electrodes, except for Adafruit 1364. The current in the case of GDH-deposited electrode should be higher as the reaction of GDH with glucose involved a cofactor $NAD(P)^+$. It reduces the NAD(P)H and H^+, resulting in higher kinetics compared to GOx,[81,82] which can be clearly seen in the case of Adafruit 1167 and 4762 since the cathodic peak voltage was almost the same for GDH- and GOx-deposited electrodes. On the contrary, the cathodic peak voltage of Adafruit 1364 for GDH electrodes is 0.1 V, which is quite lesser than that for

https://doi.org/10.1021/acsmaterialsau.4c00033
ACS Mater. Au 2024, 4, 592−603

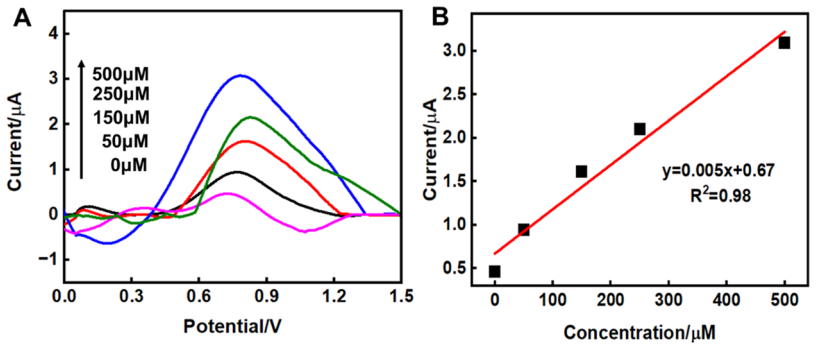

Figure 6. (A) Differential pulse voltammetry of GOx-immobilized Adafruit 1364 with 0, 0.05, 0.15, 0.25, and 0.5 mM glucose. (B) Calibration curve of GOx-immobilized Adafruit 1364 to calculate the sensitivity.

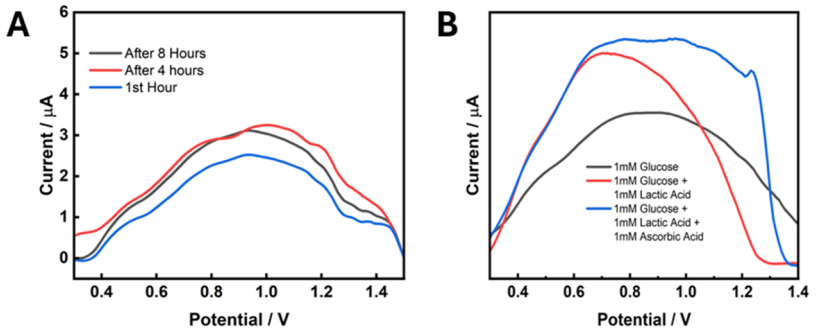

Figure 7. (A) Differential pulse voltammetry of GOx-immobilized Adafruit 1364 with 0.05 mM glucose at an interval of 4 and 8 h after storage at room temperature to check reproducibility. (B) Differential pulse voltammetry of GOx-immobilized Adafruit 1364 with 1 mM glucose (G), 1 mM lactic acid (LA), and 1 mM ascorbic Acid (AA) to study the interference effect.

GOx, which is 0.23 V, resulting in a decrease in the overall current. The figure also reveals that Adafruit 1364 exhibits the highest increase in current, signifying its potential as the most ideal material for real-time glucose monitoring applications. This outcome underscores the superior performance of the material in facilitating electron transfer and, consequently, its suitability for precision glucose sensing.

From the investigations above, since the Adafruit 1364 yielded the most favorable results, upcoming experiments on sensitivity, reproducibility, and interference were conducted using the Adafruit 1364 fabric electrode. Figures 6A and S6A display the differential pulse voltammetry curves for Adafruit 1364 with GOx and GDH immobilized, respectively, at different glucose concentrations. As the concentration of glucose varies, the corresponding peak current values change accordingly, enabling the determination of the sensitivity of the textile sensor for glucose detection using both GOx and GDH. Without any modification or addition of any additional reagents like conductive materials such as reduced graphene oxide, metallic nanoparticles to increase the conductivity of the fabric, or using any cofactor with enzymes like NAD+/NADP+ (specifically for GDH) for enhancing the reaction of the enzyme with glucose, the sensitivity for GOx-deposited Adafruit 1364 was found to be 0.005 μA μM^{-1} (Figure 6B), while for GDH-immobilized electrodes, it was 0.0019 μA μM^{-1} (Figure S6B). The limit of detection was calculated to be 41.3 μM for GOx and 63.1 μM for the GDH-immobilized fabric electrode, representing the sensitivity and LOD both being better for the GOx-immobilized Adafruit 1364 fabric electrode. The reproducibility of the Adafruit 1364 fabric electrode was tested by conducting the DPV with 0.05 mM glucose. For the GOx-immobilized fabric electrode (Figure 7A), the peak currents for 0.05 mM glucose were found to be 2.52, 3.13, and 3.06 μA with a standard deviation of current of 0.33 μA. On the contrary, 1.54, 1.92, and 1.58 μA peak current and 0.20 μA standard deviation were found for the GDH-immobilized fabric (Figure S7A), representing that both GOx- and GDH-immobilized fabric electrodes exhibited almost similar currents over time and can be used after 8 h of keeping at room temperature. Additionally, the interference from different biologically available molecules present in sweat[83] was studied by adding 1 mM lactic acid and 1 mM ascorbic acid with 1 mM glucose. In both GOx- and GDH-immobilized Adafruit 1364 fabric electrodes (Figure 7B for the GOx-immobilized fabric electrode and Figure S7B for the GDH-immobilized fabric electrode), it is observed that there was a change in current and a shift in peak potential due to the addition of lactic acid and ascorbic acid. Lactic acid and ascorbic acid are electroactive compounds and can be oxidized or reduced at the electrode surface easily in a given potential range, competing with glucose for electron transfer.[84,85] Owing to this reason, this should have resulted in the enlargement of the current and slight shift of the peak potential. This interference study indicates that there is a wide scope for modification of the fabric electrode to enhance its specificity. Applying selective coatings or membranes, such as Nafion, chitosan, or other selective polymers can help exclude interferents, while allowing glucose to reach the electrode.[86,87] Additionally, advanced signal processing techniques, including differential measurements or algorithms, can be implemented to distinguish between glucose signals and interference effects, thereby improving the accuracy.

3.3.1. Evaluation of Enzyme Selection for Practical Wearable Application. In practical applications, GDH

https://doi.org/10.1021/acsmaterialsau.4c00033
ACS Mater. Au 2024, 4, 592−603

exhibits less specificity for glucose compared to GOx.[81] Additionally, GOx does not require the immobilization of a cofactor, such as NADH, making it more convenient for use in glucose detection. Consequently, GOx is widely utilized in commercial glucose monitoring devices and is also suitable for wearable applications. Incorporating GOx into Adafruit 1364 could therefore provide a viable option for developing wearable textile-based glucose sensors.

4. SUMMARY AND CONCLUSIONS

In this research, we investigated the potential of commercially available, low-cost e-textiles for the scalable and effective development of wearable glucose biosensors. Utilizing the three distinct conductive textiles Adafruit 1364, Adafruit 1167, and Adafruit 4762, we conducted a series of comparative analyses to evaluate their suitability for integrating glucose-sensitive bioreceptors, specifically glucose oxidase and glucose dehydrogenase. These textiles were evaluated based on their morphological, electrochemical, and wearable properties through methods such as cyclic voltammetry and chronoamperometry.

Our findings revealed that Adafruit 1364 exhibited superior performance in terms of electrochemical responsiveness, flexibility, and surface absorption, which are critical for effective glucose detection and continuous wearability. Notably, Adafruit 1364 demonstrated a significant increase in current response when interfaced with glucose bioreceptors, affirming its high sensitivity and rapid signal transduction capabilities. Among two glucose-specific enzymes GOx and GDH, the Adafruit 1364 fabric electrode with GOx immobilized exhibited better performance compared to the GDH-immobilized fabric electrode, having higher sensitivity and lower LOD. The reproducibility and interference effect were also studied through DPV where both the enzyme GOx- and GDH-immobilized fabric electrode exhibited good performance in reproducibility, and a wide scope of modification has been found to increase the specificity. This makes it a potential fabric material for incorporation into wearable glucose-monitoring systems, which could provide a real-time, noninvasive approach for measuring sweat glucose levels, thereby offering a novel solution for health monitoring applications.

Furthermore, the study highlighted the importance of optimizing the textile's mechanical properties to enhance the user comfort and sensor durability, ensuring the sensor's operational stability during daily wear. The integration of such textile-based sensors into everyday garments could transform how physiological data are collected, providing a seamless and comfortable user experience.

In conclusion, the scalable application of Adafruit 1364 for glucose monitoring via e-textiles presents a promising avenue for advancing wearable health technologies. This approach could significantly impact the field of medical diagnostics and open new pathways for the development of multifunctional, smart, and wearable devices. Future work will aim to refine these technologies to enhance their applicability and reliability in diverse environmental conditions and for various physiological monitoring applications.

ASSOCIATED CONTENT

Supporting Information

The Supporting Information is available free of charge at https://pubs.acs.org/doi/10.1021/acsmaterialsau.4c00033.

Literature survey on textile-based glucose sensors, electrochemical impedance spectroscopy circuit-fitted parameters, weight concentration percentage mapping of the used materials using energy dispersive X-ray spectroscopy, corrosion of Adafruit 4762 after cyclic voltammetry, root of scan rate vs peak current of all materials to validate the Randles−Sevcik equation, tensile strength data of all materials, cyclic voltammetry of all fabrics and the standard silver electrode for chronoamperometry, differential pulse voltammetry of the GDH-immobilized fabric electrode with different concentrations of glucose (0, 0.05, 0.15, 0.25, and 0.5 mM), and DPV data for reproducibility and interferent study (PDF)

AUTHOR INFORMATION

Corresponding Author

Richa Pandey − *Department of Biomedical Engineering and Hotchkiss Brain Institute, University of Calgary, Calgary T2N 1N4 Alberta, Canada;* orcid.org/0000-0001-5070-0353; Email: richa.pandey@ucalgary.ca

Authors

Moshfiq-Us-Saleheen Chowdhury − *Department of Electrical and Software Engineering, University of Calgary, Calgary, Alberta T2N 1N4, Canada;* orcid.org/0000-0001-9562-5916

Sutirtha Roy − *Department of Electrical and Software Engineering, University of Calgary, Calgary, Alberta T2N 1N4, Canada;* orcid.org/0009-0008-8952-886X

Krishna Prasad Aryal − *Department of Biomedical Engineering, University of Calgary, Calgary T2N 1N4 Alberta, Canada*

Henry Leung − *Department of Electrical and Software Engineering, University of Calgary, Calgary, Alberta T2N 1N4, Canada*

Complete contact information is available at: https://pubs.acs.org/10.1021/acsmaterialsau.4c00033

Author Contributions

M.-U.-S.C.: conceptualization, experimentation, analysis, paper drafting, and editing. S.R.: conceptualization, chronoamperometry, conductivity experimentation, and reviewing. K.P.A.: trainee supervision, design, analysis, reviewing, and editing. H.L.: overall project supervision, funding, and reviewing. R.P.: overall project supervision, conceptualization, design, analysis, funding, editing, and reviewing. CRediT: **Moshfiq-Us-Saleheen Chowdhury** conceptualization, data curation, formal analysis, methodology, validation; **Sutirtha Roy** formal analysis, resources, writing-original draft; **Krishna Prasad Aryal** formal analysis, methodology, visualization, writing-review & editing; **Henry Leung** funding acquisition, supervision, writing-review & editing; **Richa Pandey** conceptualization, formal analysis, funding acquisition, methodology, project administration, supervision, writing-review & editing.

https://doi.org/10.1021/acsmaterialsau.4c00033
ACS Mater. Au 2024, 4, 592−603

Notes

The authors declare no competing financial interest.

■ ACKNOWLEDGMENTS

We acknowledge the following funding resources: Major Innovation Fund—Space and Defense Technologies, New Frontiers Research Fund-Exploration, NSERC DG, and Alberta Innovates, University of Calgary, and Research Excellence Chair.

■ REFERENCES

(1) Massaroni, C.; Saccomandi, P.; Schena, E. Medical smart textiles based on fiber optic technology: an overview. *J. Funct. Biomater.* **2015**, *6* (2), 204−221.
(2) Meena, J. S.; Choi, S. B.; Jung, S. B.; Kim, J. W. Electronic textiles: New age of wearable technology for healthcare and fitness solutions. *Materials Today Bio* **2023**, *19*, No. 100565.
(3) Tat, T.; Chen, G.; Zhao, X.; Zhou, Y.; Xu, J.; Chen, J. Smart textiles for healthcare and sustainability. *ACS Nano* **2022**, *16* (9), 13301−13313.
(4) Ruckdashel, R. R.; Venkataraman, D.; Park, J. H. Smart textiles: A toolkit to fashion the future. *J. Appl. Phys.* **2021**, *129* (13), No. 130903.
(5) Karpagam, K. R.; Saranya, K. S.; Gopinathan, J.; Bhattacharyya, A. Development of smart clothing for military applications using thermochromic colorants. *J. Text. Inst.* **2017**, *108* (7), 1122−1127.
(6) Devendorf, L.; Di Lauro, C.et al.Adapting double weaving and yarn plying techniques for smart textiles applications. In *Proceedings of the Thirteenth International Conference on Tangible, Embedded, and Embodied Interaction*, 2019; pp 77−85.
(7) Wu, S.; Devendorf, L.et al.Unfabricate: designing smart textiles for disassembly. In *Proceedings of the 2020 CHI Conference on Human Factors in Computing Systems* 2020; pp 1−14.
(8) Chen, Y.; Deng, Z.; Ouyang, R.; Zheng, R.; Jiang, Z.; Bai, H.; Xue, H. 3D printed stretchable smart fibers and textiles for self-powered e-skin. *Nano Energy* **2021**, *84*, No. 105866.
(9) Gashti, M. P.; Pakdel, E.; Alimohammadi, F. Nanotechnology-based coating techniques for smart textiles. In *Active Coatings for Smart Textiles*; Woodhead Publishing, 2016; pp 243−268.
(10) Singh, A.; Sharma, A.; Arya, S. Human sweat-based wearable glucose sensor on cotton fabric for real-time monitoring. *J. Anal. Sci. Technol.* **2022**, *13* (1), No. 11.
(11) Chen, C.; Ran, R.; Yang, Z.; Lv, R.; Shen, W.; Kang, F.; Huang, Z. H. An efficient flexible electrochemical glucose sensor based on carbon nanotubes/carbonized silk fabrics decorated with Pt microspheres. *Sens. Actuators, B* **2018**, *256*, 63−70.
(12) Xiao, G.; He, J.; Chen, X.; Qiao, Y.; Wang, F.; Xia, Q.; Yu, L.; Lu, Z. A wearable, cotton thread/paper-based microfluidic device coupled with smartphone for sweat glucose sensing. *Cellulose* **2019**, *26*, 4553−4562.
(13) Tabor, J.; Chatterjee, K.; Ghosh, T. K. Smart textile-based personal thermal comfort systems: current status and potential solutions. *Adv. Mater. Technol.* **2020**, *5* (5), No. 1901155.
(14) Yang, S.; Li, C.; Wen, N.; Xu, S.; Huang, H.; Cong, T.; Pan, L.; et al. All-fabric-based multifunctional textile sensor for detection and discrimination of humidity, temperature, and strain stimuli. *J. Mater. Chem. C* **2021**, *9* (39), 13789−13798.
(15) Codau, T. C.; Onofrei, E.; Bedek, G.; Dupont, D.; Cochrane, C. Embedded textile heat flow sensor characterization and application. *Sens. Actuators, A* **2015**, *235*, 131−139.
(16) Faruk, M. O.; Ahmed, A.; Jalil, M. A.; Islam, M. T.; Shamim, A. M.; Adak, B.; Hossain, M. M.; Mukhopadhyay, S. Functional textiles and composite based wearable thermal devices for Joule heating: progress and perspectives. *Appl. Mater. Today* **2021**, *23*, No. 101025.
(17) Kuzubasoglu, B. A.; Sayar, E.; Cochrane, C.; Koncar, V.; Bahadir, S. K. Wearable temperature sensor for human body temperature detection. *J. Mater. Sci.: Mater. Electron.* **2021**, *32*, 4784−4797.
(18) Zhang, J. W.; Zhang, Y.; Li, Y. Y.; Wang, P. Textile-based flexible pressure sensors: A review. *Polym. Rev.* **2022**, *62* (1), 65−94.
(19) An, J.; Ma, Y.; He, M.; Yan, J.; Zhang, C.; Li, X.; Gao, Y.; et al. A wearable and highly sensitive textile-based pressure sensor with Ti3C2Tx nanosheets. *Sens. Actuators, A* **2020**, *311*, No. 112081.
(20) Zheng, Y.; Yin, R.; Zhao, Y.; Liu, H.; Zhang, D.; Shi, X.; Shen, C.; et al. Conductive MXene/cotton fabric-based pressure sensor with both high sensitivity and wide sensing range for human motion detection and E-skin. *Chem. Eng. J.* **2021**, *420*, No. 127720.
(21) Lim, S. J.; Bae, J. H.; Han, J. H.; Jang, S. J.; Oh, H. J.; Lee, W.; Kim, S. H.; Ko, J. H. Foldable and washable fully textile-based pressure sensor. *Smart Mater. Struct.* **2020**, *29* (5), No. 055010.
(22) Hudec, R.; Matúška, S.; Kamencay, P.; Benco, M. A smart IoT system for detecting the position of a lying person using a novel textile pressure sensor. *Sensors* **2021**, *21* (1), 206.
(23) Qi, K.; Wang, H.; You, X.; Tao, X.; Li, M.; Zhou, Y.; Cui, S.; et al. Core-sheath nanofiber yarn for textile pressure sensor with high pressure sensitivity and spatial tactile acuity. *J. Colloid Interface Sci.* **2020**, *561*, 93−103.
(24) Wang, J.; Lu, C.; Zhang, K. Textile-based strain sensor for human motion detection. *Energy Environ. Mater.* **2020**, *3* (1), 80−100.
(25) Liu, X.; Miao, J.; Fan, Q.; Zhang, W.; Zuo, X.; Tian, M.; Qu, L.; et al. Recent progress on smart fiber and textile based wearable strain sensors: materials, fabrications and applications. *Adv. Fiber Mater.* **2022**, *4* (3), 361−389.
(26) Zahid, M.; Zych, A.; Dussoni, S.; Spallanzani, G.; Donno, R.; Maggiali, M.; Athanassiou, A. Wearable and self-healable textile-based strain sensors to monitor human muscular activities. *Composites, Part B* **2021**, *220*, No. 108969.
(27) Luo, C.; Tian, B.; Liu, Q.; Feng, Y.; Wu, W. One-step-printed, highly sensitive, textile-based, tunable performance strain sensors for human motion detection. *Adv. Mater. Technol.* **2020**, *5* (2), No. 1900925.
(28) Liu, Z.; Zhu, T.; Wang, J.; Zheng, Z.; Li, Y.; Li, J.; Lai, Y. Functionalized fiber-based strain sensors: pathway to next-generation wearable electronics. *Nano-Micro Lett.* **2022**, *14* (1), No. 61.
(29) Rauf, S.; Vijjapu, M. T.; Andrés, M. A.; Gascón, I.; Roubeau, O.; Eddaoudi, M.; Salama, K. N. Highly selective metal−organic framework textile humidity sensor. *ACS Appl. Mater. Interfaces* **2020**, *12* (26), 29999−30006.
(30) Su, Y.; Liu, Y.; Li, W.; Xiao, X.; Chen, C.; Lu, H.; Chen, J.; et al. Sensing−transducing coupled piezoelectric textiles for self-powered humidity detection and wearable biomonitoring. *Mater. Horiz.* **2023**, *10* (3), 842−851.
(31) Hatamie, A.; Angizi, S.; Kumar, S.; Pandey, C. M.; Simchi, A.; Willander, M.; Malhotra, B. D. Review—Textile based chemical and physical sensors for healthcare monitoring. *J. Electrochem. Soc.* **2020**, *167* (3), No. 037546.
(32) Gualandi, I.; Tessarolo, M.; Mariani, F.; Possanzini, L.; Scavetta, E.; Fraboni, B. Textile chemical sensors based on conductive polymers for the analysis of sweat. *Polymers* **2021**, *13* (6), 894.
(33) Islam, G. M. N.; Ali, A.; Collie, S. Textile sensors for wearable applications: A comprehensive review. *Cellulose* **2020**, *27*, 6103−6131.
(34) Qureshi, S.; Stojanović, G. M.; Simić, M.; Jeoti, V.; Lashari, N.; Sher, F. Silver conductive threads-based embroidered electrodes on textiles as moisture sensors for fluid detection in biomedical applications. *Materials* **2021**, *14* (24), 7813.
(35) Tseghai, G. B.; Malengier, B.; Fante, K. A.; Nigusse, A. B.; Van Langenhove, L. Integration of conductive materials with textile structures, an overview. *Sensors* **2020**, *20* (23), 6910.
(36) Ouyang, Z.; Xu, D.; Yu, H. Y.; Li, S.; Song, Y.; Tam, K. C. Novel ultrasonic-coating technology to design robust, highly sensitive and wearable textile sensors with conductive nanocelluloses. *Chem. Eng. J.* **2022**, *428*, No. 131289.
(37) Marra, F.; Minutillo, S.; Tamburrano, A.; Sarto, M. S. Production and characterization of Graphene Nanoplatelet-based

https://doi.org/10.1021/acsmaterialsau.4c00033
ACS Mater. Au 2024, 4, 592−603

ink for smart textile strain sensors via screen printing technique. *Mater. Des.* **2021**, *198*, No. 109306.
(38) Lee, S. W.; Jung, H. G.; Jang, J. W.; Park, D.; Lee, D.; Kim, I.; Yoon, D. S.; et al. Graphene-based electronic textile sheet for highly sensitive detection of NO2 and NH3. *Sens. Actuators, B* **2021**, *345*, No. 130361.
(39) Afroj, S.; Tan, S.; Abdelkader, A. M.; Novoselov, K. S.; Karim, N. Highly conductive, scalable, and machine washable graphene-based E-textiles for multifunctional wearable electronic applications. *Adv. Funct. Mater.* **2020**, *30* (23), No. 2000293.
(40) Rajan, G.; Morgan, J. J.; Murphy, C.; Torres Alonso, E.; Wade, J.; Ott, A. K.; Neves, A. I.; et al. Low operating voltage carbon−graphene hybrid E-textile for temperature sensing. *ACS Appl. Mater. Interfaces* **2020**, *12* (26), 29861−29867.
(41) Shathi, M. A.; Chen, M.; Khoso, N. A.; Rahman, M. T.; Bhattacharjee, B. Graphene coated textile based highly flexible and washable sports bra for human health monitoring. *Mater. Des.* **2020**, *193*, No. 108792.
(42) Ergoktas, M. S.; Bakan, G.; Steiner, P.; Bartlam, C.; Malevich, Y.; Ozden-Yenigun, E.; Kocabas, C.; et al. Graphene-enabled adaptive infrared textiles. *Nano Lett.* **2020**, *20* (7), 5346−5352.
(43) Zhu, J.; El Nesr, N.; Simon, C.; Rettenmaier, N.; Beiler, K.; Kao, C. H. L. BioWeave: Weaving Thread-Based Sweat-Sensing On-Skin Interfaces. *Proceedings of the 36th Annual ACM Symposium on User Interface Software and Technology* **2023**, 1−11.
(44) Chatterjee, K.; Ghosh, T. K. 3D printing of textiles: potential roadmap to printing with fibers. *Adv. Mater.* **2020**, *32* (4), No. 1902086.
(45) Kalkal, A.; Kumar, S.; Kumar, P.; Pradhan, R.; Willander, M.; Packirisamy, G.; Kumar, S.; Malhotra, B. D. Recent advances in 3D printing technologies for wearable (bio) sensors. *Addit. Manuf.* **2021**, *46*, No. 102088.
(46) Shah, M. A.; Pirzada, B. M.; Price, G.; Shibiru, A. L.; Qurashi, A. Applications of nanotechnology in smart textile industry: A critical review. *J. Adv. Res.* **2022**, *38*, 55−75.
(47) Barman, J.; Tirkey, A.; Batra, S.; Paul, A. A.; Panda, K.; Deka, R.; Babu, P. J. The role of nanotechnology based wearable electronic textiles in biomedical and healthcare applications. *Mater. Today Commun.* **2022**, *32*, No. 104055.
(48) Chen, G.; Xiao, X.; Zhao, X.; Tat, T.; Bick, M.; Chen, J. Electronic textiles for wearable point-of-care systems. *Chem. Rev.* **2022**, *122* (3), 3259−3291.
(49) Zaman, S. U.; Tao, X.; Cochrane, C.; Koncar, V. Smart E-textile systems: a review for healthcare applications. *Electronics* **2022**, *11* (1), 99.
(50) Blachowicz, T.; Ehrmann, G.; Ehrmann, A. Textile-based sensors for biosignal detection and monitoring. *Sensors* **2021**, *21* (18), 6042.
(51) Kubicek, J.; Fiedorova, K.; Vilimek, D.; Cerny, M.; Penhaker, M.; Janura, M.; Rosicky, J. Recent trends, construction, and applications of smart textiles and clothing for monitoring of health activity: A comprehensive multidisciplinary review. *IEEE Rev. Biomed. Eng.* **2022**, *15*, 36−60.
(52) Alizadeh Meghrazi, M.; Tian, Y.; Mahnam, A.; Bhattachan, P.; Eskandarian, L.; Taghizadeh Kakhki, S.; Popovic, M. R.; Lankarany, M. Multichannel ECG recording from waist using textile sensors. *BioMed. Eng. OnLine* **2020**, *19* (1), No. 48.
(53) Di Tocco, J.; Raiano, L.; Sabbadini, R.; Massaroni, C.; Formica, D.; Schena, E. A wearable system with embedded conductive textiles and an imu for unobtrusive cardio-respiratory monitoring. *Sensors* **2021**, *21* (9), 3018.
(54) Issatayeva, A.; Beisenova, A.; Tosi, D.; Molardi, C. Fiber-optic based smart textiles for real-time monitoring of breathing rate. *Sensors* **2020**, *20* (12), 3408.
(55) Su, Y.; Ma, C.; Chen, J.; Wu, H.; Luo, W.; Peng, Y.; Li, H.; et al. Printable, highly sensitive flexible temperature sensors for human body temperature monitoring: a review. *Nanoscale Res. Lett.* **2020**, *15*, No. 200.
(56) García Patiño, A.; Khoshnam, M.; Menon, C. Wearable device to monitor back movements using an inductive textile sensor. *Sensors* **2020**, *20* (3), 905.
(57) Zhou, X.; Hu, C.; Lin, X.; Han, X.; Zhao, X.; Hong, J. Polyaniline-coated cotton knitted fabric for body motion monitoring. *Sens. Actuators, A* **2021**, *321*, No. 112591.
(58) Teymourian, H.; Moonla, C.; Tehrani, F.; Vargas, E.; Aghavali, R.; Barfidokht, A.; Wang, J.; et al. Microneedle-based detection of ketone bodies along with glucose and lactate: toward real-time continuous interstitial fluid monitoring of diabetic ketosis and ketoacidosis. *Anal. Chem.* **2020**, *92* (2), 2291−2300.
(59) García-Guzmán, J. J.; Pérez-Ràfols, C.; Cuartero, M.; Crespo, G. A. Microneedle based electrochemical (Bio)Sensing: Towards decentralized and continuous health status monitoring. *TrAC, Trends Anal. Chem.* **2021**, *135*, No. 116148.
(60) Myers, M. G., Jr.; Affinati, A. H.; Richardson, N.; Schwartz, M. W. Central nervous system regulation of organismal energy and glucose homeostasis. *Nat. Metab.* **2021**, *3* (6), 737−750.
(61) Chen, C.; Ran, R.; Yang, Z.; Lv, R.; Shen, W.; Kang, F.; Huang, Z. H. An efficient flexible electrochemical glucose sensor based on carbon nanotubes/carbonized silk fabrics decorated with Pt microspheres. *Sens. Actuators, B* **2018**, *256*, 63−70.
(62) Xiao, G.; He, J.; Chen, X.; Qiao, Y.; Wang, F.; Xia, Q.; Yu, L.; Lu, Z. A wearable, cotton thread/paper-based microfluidic device coupled with smartphone for sweat glucose sensing. *Cellulose* **2019**, *26*, 4553−4562.
(63) Norrod, K. L.; Sudnik, L. M.; Rousell, D.; Rowlen, K. L. Quantitative comparison of five SERS substrates: sensitivity and limit of detection. *Appl. Spectrosc.* **1997**, *51* (7), 994−1001.
(64) Long, G. L.; Winefordner, J. D. Limit of detection. A closer look at the IUPAC definition. *Anal. Chem.* **1983**, *55* (7), 712A−724A.
(65) Sun, L.; Tian, C.; Fu, Y.; Yang, Y.; Yin, J.; Wang, L.; Fu, H. Nitrogen-doped porous graphitic carbon as an excellent electrode material for advanced supercapacitors. *Chem. − Eur. J.* **2014**, *20* (2), 564−574.
(66) Randles, J. E. B. A cathode ray polarograph. Part II. —The current-voltage curves. *Trans. Faraday Soc.* **1948**, *44*, 327−338.
(67) (a) Sevcik, A. Collection Czechoslov. *Chem. Commun.* **1947**, *13* (349), 1948. (b) JEB I~ ANDLES. *Disc. Faraday Soc. 1*, 11.
(68) Li, Y.; Meng, Y.; Xiao, M.; Liu, X.; Zhu, F.; Zhang, Y. The surface capacitance behavior and its contribution to the excellent performance of cobalt ferrite/carbon anode in lithium storage. *J. Mater. Sci.: Mater. Electron.* **2019**, *30*, 12659−12668.
(69) Upasham, S.; Banga, I. K.; Jagannath, B.; Paul, A.; Lin, K. C.; Muthukumar, S.; Prasad, S. Electrochemical impedimetric biosensors, featuring the use of Room Temperature Ionic Liquids (RTILs): Special focus on non-faradaic sensing. *Biosens. Bioelectron.* **2021**, *177*, No. 112940.
(70) Kumar, N.; Arora, A.; Krishnan, A. Complementary AC Voltammetry—A Method for Simultaneous Measurement of Faradaic and Nonfaradaic Currents in an Electrochemically Reversible System. *IEEE Sens. J.* **2020**, *20* (22), 13196−13203.
(71) Adamu, B. F.; Gao, J. Comfort related woven fabric transmission properties made of cotton and nylon. *Fashion Text.* **2022**, *9* (1), No. 8.
(72) Jhanji, Y.; Gupta, D.; Kothari, V. K. Thermo-physiological properties of polyester−cotton plated fabrics in relation to fibre linear density and yarn type. *Fashion Text.* **2015**, *2* (1), No. 16.
(73) Fiorito, P. A.; Torresi, S. I. Glucose amperometric biosensor based on the co-immobilization of glucose oxidase (GOx) and ferrocene in poly (pyrrole) generated from ethanol/water mixtures. *J. Braz. Chem. Soc.* **2001**, *12*, 729−733.
(74) Raba, J.; Mottola, H. A. Glucose oxidase as an analytical reagent. *Crit. Rev. Anal. Chem.* **1995**, *25* (1), 1−42.
(75) Ferri, S.; Kojima, K.; Sode, K. Review of glucose oxidases and glucose dehydrogenases: a bird's eye view of glucose sensing enzymes. *J. Diabetes Sci. Technol.* **2011**, *5* (5), 1068−1076.

https://doi.org/10.1021/acsmaterialsau.4c00033
ACS Mater. Au 2024, 4, 592−603

(76) Zhang, M.; Mullens, C.; Gorski, W. Coimmobilization of dehydrogenases and their cofactors in electrochemical biosensors. *Anal. Chem.* **2007**, *79* (6), 2446−2450.
(77) Pal, T.; Narayanan, V. A.; Stokes, D. L.; Vo-Dinh, T. Surface-enhanced Raman detection of nicotinamide in vitamin tablets. *Anal. Chim. Acta* **1998**, *368* (1−2), 21−28.
(78) Sinha, B.; Sarkar, B. K.; Roy, M. N. Apparent molar volumes and viscosity B-coefficients of nicotinamide in aqueous tetrabutylammonium bromide solutions at T = (298.15, 308.15, and 318.15) K. *J. Chem. Thermodyn.* **2008**, *40* (3), 394−400.
(79) Osterman, A. Biogenesis and homeostasis of nicotinamide adenine dinucleotide cofactor. *EcoSal Plus* **2009**, *3* (2), 10−1128.
(80) Corpas, F. J.; González-Gordo, S.; Palma, J. M. Nitric oxide and hydrogen sulfide modulate the NADPH-generating enzymatic system in higher plants. *J. Exp. Bot.* **2021**, *72* (3), 830−847.
(81) Öberg, D.; Östenson, C. G. Performance of glucose dehydrogenase−and glucose oxidase−based blood glucose meters at high altitude and low temperature. *Diabetes Care* **2005**, *28* (5), 1261.
(82) German, N.; Popov, A.; Ramanavicius, A.; Ramanaviciene, A. Development and practical application of glucose biosensor based on dendritic gold nanostructures modified by conducting polymers. *Biosensors* **2022**, *12* (8), 641.
(83) Xu, J.; Fang, Y.; Chen, J. Wearable biosensors for non-invasive sweat diagnostics. *Biosensors* **2021**, *11* (8), 245.
(84) Shao, W.; Mai, J.; Wei, Z. Nonenzymatic lactic acid detection using cobalt polyphthalocyanine/carboxylated multiwalled carbon nanotube nanocomposites modified sensor. *Chemosensors* **2022**, *10* (2), 83.
(85) Argoubi, W.; Rabti, A.; Aoun, S. B.; Raouafi, N. Sensitive detection of ascorbic acid using screen-printed electrodes modified by electroactive melanin-like nanoparticles. *RSC Adv.* **2019**, *9* (64), 37384−37390.
(86) Myndrul, V.; Iatsunskyi, I.; Babayevska, N.; Jarek, M.; Jesionowski, T. Effect of electrode modification with chitosan and nafion on the efficiency of real-time enzyme glucose biosensors based on ZnO tetrapods. *Materials* **2022**, *15* (13), 4672.
(87) Thuy, T. N. T.; Tseng, T. T. C. A micro-platinum wire biosensor for fast and selective detection of alanine aminotransferase. *Sensors* **2016**, *16* (6), 767.

https://doi.org/10.1021/acsmaterialsau.4c00033
ACS Mater. Au 2024, 4, 592−603